STScI | SPACE TELESCOPE SCIENCE INSTITUTE

Instrument Science Report WFC3 2024-01

Sensitivity Evolution of WFC3/IR Using Spatial Scanning Photometry and Grism Spectrophotometry

D. Som, R. Bohlin, J. Mack, V. Bajaj, A. Calamida

March 22, 2024

Abstract

Spatial scanning and slitless spectroscopic observations with the Wide Field Camera 3 (WFC3) IR channel are used to quantify its photometric stability and provide independent estimates of the rate of sensitivity evolution. Spatial scans of stars in the open cluster M35 observed with the F140W filter reveal a sensitivity loss at the rate of 0.065 ± 0.006 % per year and also result in the first measurement of a sensitivity loss of 0.157 ± 0.021 % per year in the F098M filter. Observations of spectrophotometric standard stars with the WFC IR grisms, G102 and G141, demonstrate photometric sensitivity losses at the annual rates of 0.115 ± 0.008 % yr^{-1} and 0.061 ± 0.007 % yr^{-1}, respectively. The imaging and the grism modes of WFC3/IR show similar sensitivity evolution over comparable wavelength ranges.

1 Introduction

The infrared channel of the Wide Field Camera 3 (WFC3/IR), with its 15 narrow, medium, and broad band filters and 2 grisms (G102, G141), is heavily used for a variety of science applications: from solar system and exoplanet studies to galaxy evolution and cosmology. Therefore, characterizing and monitoring the photometric stability of WFC3/IR is of critical importance to its optimal and scientifically impactful usage.

The performance of WFC3's IR channel has been monitored since the time of its commissioning in 2009, primarily through 'staring mode' (fixed pointing during the length of an

exposure) observations of spectrophotometric standard stars. In one of the earliest studies utilizing the first ∼1.5 years of on-sky data, Kalirai, *et al.* (2011) did not find any significant sensitivity evolution but reported a 1-σ photometric repeatability of $\sim$ 1 %. Bajaj, *et al.* (2020) analyzed standard star data obtained between 2009–2020 through various non-grism filters and did not detect any evolution in the WFC3/IR sensitivity. This study also argued that the observed limit of $\sim$ 1 % in the repeatability of photometric measurements could potentially mask any subtle long-term trend in sensitivity. On the other hand, Kozhurina-Platais & Baggett, (2020) analyzed F160W observations of stars in the core of the globular cluster Omega Centauri (ω-Cen) via PSF photometry and found the sensitivity to evolve at the rate of $\sim$ -0.2% yr^{-1}. Subsequently, Bajaj, *et al.* (2022) reported a sensitivity loss of 0.13 $\pm$ 0.02% yr^{-1}, estimated from stellar photometry in the outer regions of Messier 4, 47 Tucanae & ω-Cen and found no apparent wavelength dependence of this evolution.

One of the leading factors limiting photometric stability studies is the photometric precision achieved from staring mode imaging observations. Since 2015, WFC3/IR photometric calibration efforts have started utilizing the spatial scanning technique (McCullough & MacKenty, 2012), which by letting the target drift slowly across the detector during an exposure spreads out photons along the scan length. This allows a large number of photons from relatively bright sources to be collected without significant saturation, and increases measurement precision by reducing the Poisson noise. Som, *et al.* (2021), S21 hereafter, used scanned images of Messier 35 (M35) obtained between 2015–2021 to provide the first spatial scanning based measurement of WFC3/IR's sensitivity evolution. This study reported a weak sensitivity evolution of -0.024 $\pm$ 0.008% yr^{-1} and a short-term 1-σ photometric repeatability of $\gtrsim$ 0.65% from F140W observations, but was unable to detect any evolution using only two epochs (separated by ∼1 year) of F098M observations.

Another probe of the photometric stability of WFC3/IR is provided by grism observations, which, similar to spatial scans, spread source photons on the detector. Spectrophotometric observations with G102 and G141 have long been used to monitor the photometric performance of this observing mode. Bohlin & Deustua (2019) used observations of several CALSPEC standard stars acquired between 2009–2018 to report photometric sensitivity loss rates of 0.169 $\pm$ 0.015% yr^{-1} and 0.085 $\pm$ 0.014% yr^{-1} for G102 and G141, respectively.

Using the most complete sets of scanned imaging and grism observations as of this writing, this work investigates the long-term stability of WFC3/IR photometric performance and presents updated estimates of the sensitivity evolution. This report is structured as follows: the spatial scanning analysis is presented in Section 2 with Sections 2.1 and 2.2 describing the data and analysis methods used, respectively. Section 2.3 presents the results of the spatial scanning analysis. Section 3 presents results for the staring mode spectrophotometry with the G102 and G141 grisms. Finally, Section 4 summarizes this work and discusses avenues for future work.

2 Scanned Imaging Photometry

2.1 Data

Spatial scanning observations of stars in the open cluster M35, obtained using F098M (bandpass: 900–1070 nm) and F140W (bandpass: 1200-1600 nm) as part of calibration programs 14020, 16031, 16439, and 17261, were used to quantify the photometric sensitivity evolution of WFC3/IR. Program 14020 targeted a field in M35 containing a loose group of bright and photometrically stable stars for scanned imaging with F140W. These observations were distributed over 4 epochs between January - April 2015 with a cadence of ∼1 month between the successive 1-orbit visits. The same M35 field was targeted by program 16031 over 2 visits, each containing an orbit with F140W and F098M observations, and executed 1 year apart in January 2020 and January 2021. The only difference in the F140W observation structure between these two programs is in the extent of dithers; the pattern used in the latter program sampled the detector more extensively in comparison with the 2015 data. Programs 16439 and 17261 were identical to 16031 in their observation strategy except that the two epochs of observation in each of these programs were executed ∼3 months apart, in 2022 and 2023, respectively. All exposures, irrespective of the filter, were spatially scanned forward at 0.76 degrees at a rate of 1.5 arcsec/sec for a total exposure time of ∼ 8.8 seconds (`SAMP-SEQ=SPARS10, NSAMP=2`), and used the `512 x 512` sub-array readout at the center of the IR detector.

Star ID	RA (ICRS J2000)	Dec (ICRS J2000)	J_{Mag}	Variability (mag)
1	06:09:03.50	+24:21:35.0	11.6	0.0008
2	06:09:04.46	+24:21:54.7	11.7	0.0009
3	06:09:02.92	+24:21:53.4	11.1	0.0002
4	06:09:02.18	+24:22:27.5	10.2	0.0006
5	06:09:00.02	+24:22:25.9	11.2	0.0005
X	06:08:59.61	+24:21:59.5	10.3	0.0085

Table 1: *Stars in the targeted M35 field used in this scanned imaging analysis. Stellar flux variability is from a month of monitoring with Kepler/K2 and was provided by Andrew Vanderburg (private communication). Scans from stars 1, 2, 3, and 4 were used in the analysis of F140W data while stars 3, 4, and 5 were used to analyze F098M scans. The last row with ID 'X' lists a pulsating variable star which was included in the F098M scanned imaging analysis by S21 but has been excluded from this work due to its high intrinsic variability.*

The F140W data are distributed over 10 epochs spanning a ∼ 8-year baseline between 2015 and 2023. Observations with F098M from programs 16031, 16439, and 17261 span a shorter baseline of 3 years, spread over 4 epochs between 2020 and 2023. Observations presented here include scans from several stars in the targeted M35 field but the number varies between exposures as a result of dithering. For analyzing data taken with each filter, a set of bright ($J_{mag} < 12$) stars with low 1-σ variability (≤ 0.0009 mag) in the Kepler/K2

bandpass and having the highest number of complete scans in the full dataset were identified. Table 1 lists the stars in M35 included in our spatial scanning analysis. Please note that, as a result of the selection described above, different sets of stellar scans were analyzed for F140W and F098M, with only 2 stars common between them. Figure 1 presents examples of scanned images analyzed with F098M and F140W.

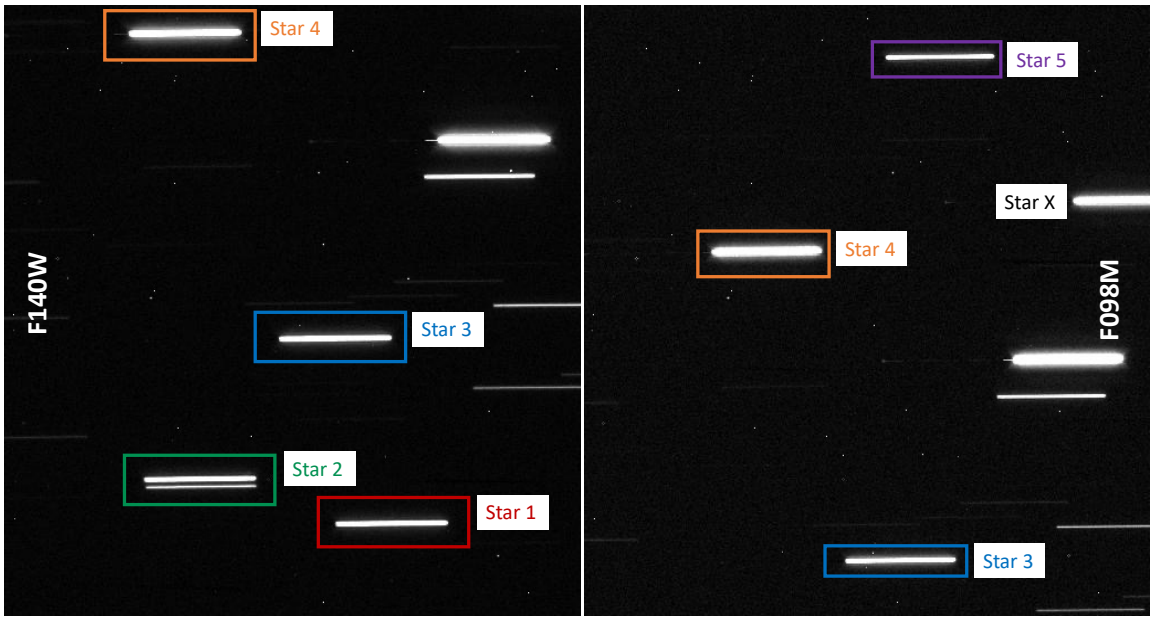

Figure 1: *Left: M35 stellar scans used in the analysis of the F140W photometry. Right: M35 stellar scans used in the analysis of the F098M photometry. Different sets of scans were used for the analysis of F140W and F098M data, with 'Star 3' and 'Star 4' common to both sets. The scan marked as 'Star X' in the F098M image is from a pulsating variable star (see also Table 1) which was included in the analysis by S21 but has been excluded from this work due to its high intrinsic variability.*

2.2 Photometry of Spatial Scans

Analyzing the scanned images to quantify sensitivity evolution of WFC3/IR essentially involves aperture photometry of stellar scans and estimating how the measurements evolve with time. This work adopts the `Python 3` based analysis framework established and described in details by S21, and a summary of the process is given below.

The raw data were processed using the WFC3 calibration pipeline, `calwf3 v3.6.1`, utilizing the latest reference files including updated flatfields (`PFLT` and `DFLT` files, see Mack et al. 2021, and Olszewski & Mack, 2021). The accumulated counts from the last readout of the pipeline-generated `IMA` files were used in our analysis. Count-rates from the `FLT` files were not considered because the up-the-ramp fitting could be sensitive to non-uniformity in scan rates and may not be accurate.

The IMA images were corrected for geometric distortions by multiplying with the WFC3/IR pixel-area map, 'ir_wfc3_map.fits'[1], and then used to measure flux in stellar scans using rectangular apertures. The dimensions of an aperture used to measure scans from a given star were optimized so that the aperture fully contains the scans but is not too large to introduce additional noise. Table 2 lists the aperture dimensions, determined separately for each stellar scan in a given filter. Following S21, this work adopts an automated aperture centering mechanism which centers apertures in pixel space around scans in a reference image, converts the center coordinates into RA and Dec via the reference image's WCS information, and finally, re-positions these apertures on any other image by converting the RA and Dec coordinates back into pixel space via the second image's WCS information. Each aperture was also accompanied by a rectangular annulus used to sample the sky-background. These annular apertures too, were also tailored for each star and had the same centers as the corresponding scan apertures. Their dimensions were chosen to provide a large enough area to measure the background without significant contamination from other scans. Given all observations used in this work use the same scan rate and exposure times, measurement consistency was ensured by using the same aperture dimensions to measure a given star in all images from the same filter. Figures 2a and 2b show the apertures and the corresponding background regions used to analyze F140W and F098M data, respectively.

Star	F140W Apertures		F098M Apertures	
	Width	Height	Width	Height
	(arcsec)	(arcsec)	(arcsec)	(arcsec)
1	16.00	5.00	...	...
2	16.00	5.00	...	...
3	16.50	5.00	16.50	5.00
4	16.50	5.50	16.00	5.50
5	...	...	16.00	5.00

Table 2: *Aperture dimensions used for measuring stellar scans from the F140W and F098M data used in this work.*

Using the apertures described above and various modules available in wfc3_photometry [2] and photutils[3] packages, total counts were measured from the stellar scans and the corresponding Poisson errors were estimated. The mean pixel value within the corresponding background aperture provided a measure of the typical local background in each pixel which was then scaled by the area of the photometric aperture to estimate the total background. This background was then subtracted from the measured flux and the errors were propagated appropriately.

Finally, the measurements were filtered to discard scans which were located close to the detector edges resulting in the loss of a significant fraction of their background apertures.

[1]https://www.stsci.edu/hst/instrumentation/wfc3/data-analysis/pixel-area-maps

[2]https://github.com/spacetelescope/wfc3_photometry

[3]Bradley, L. et al. (2017). astropy/photutils: v0.4. doi: 10.5281/zenodo.1039309. url: https://doi.org/10.5281/zenodo.1039309

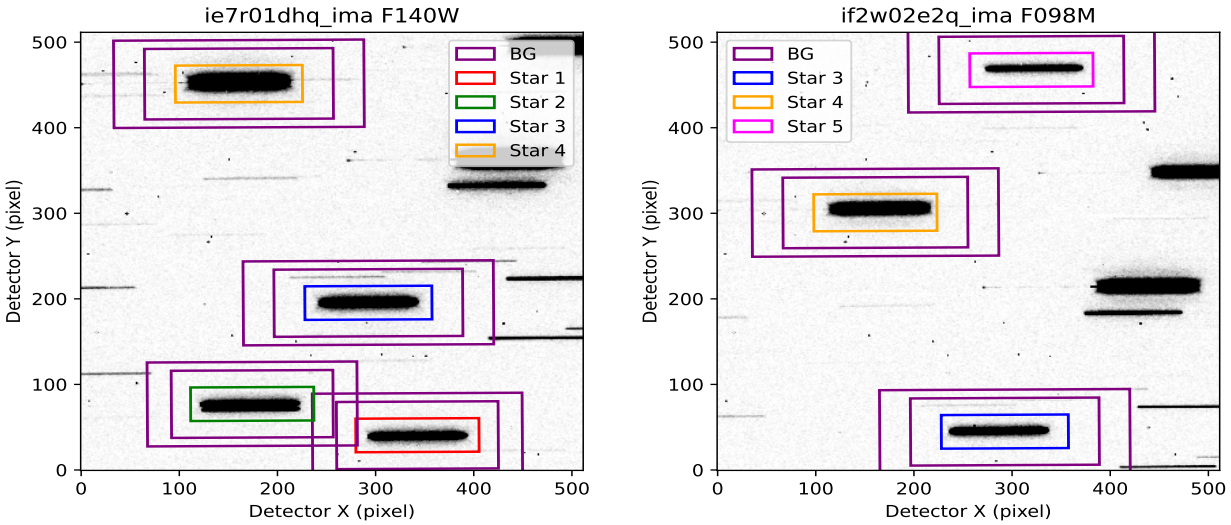

(a) (b)

Figure 2: *(a): The apertures and the corresponding background regions used for measuring the stellar scans in F140W. The aperture measuring star i is marked as 'Star i' where i = 1, 2, 3, or 4. The color scheme used to mark these apertures is carried forward through the following plots presenting measurements from the corresponding stars. (b): Same as Fig. 2a but for measurements with F098M data. The aperture measuring star i is marked as 'Star i' where i = 3, 4, or 5. Star 3 and Star 4 are common to both filters.*

'Buffer' regions along the detector edges were estimated based on the typical scan length and/or background region dimensions, and scans with centers within ∼30 (60) pixels of the left/right (top/bottom) edges were excluded from further analysis.

2.3 Time-dependence of Sensitivity

Measurements from different epochs were combined to investigate the long term photometric stability of the WFC3/IR imaging mode. We use relative photometry of the stars in our sample, obtained by normalizing individual measurements from a star by the mean of all its measurements from a given filter, to quantify the time-dependence of photometric sensitivity.

Spatial scanning observations obtained over 10 epochs between 2015 and 2023 were used to estimate the time dependence of WFC3/IR imaging mode sensitivity in F140W. Figure 3a shows the relative photometry derived from measurements made over the ∼ 8 year baseline. A linear fit to the data reveals a loss of sensitivity at the rate of 0.065 ± 0.006% yr^{-1}, ∼ 2.7 times higher than the loss rate discovered by S21 using F140W spatial scanning observations spanning a ∼ 6 year baseline. The data obtained with F098M between 2020 and 2023 are presented in Figure 3b) and provide the first estimate of sensitivity evolution in this filter at a rate of -0.157 ± 0.021% per year. It is to be noted that the evolution rate, when determined from a small number of epochs over a short baseline, could be susceptible to bias from inter-epoch photometric fluctuations (see, e.g., S21), and this measurement instability should recede as the number of epochs increases over an expanding baseline. Therefore,

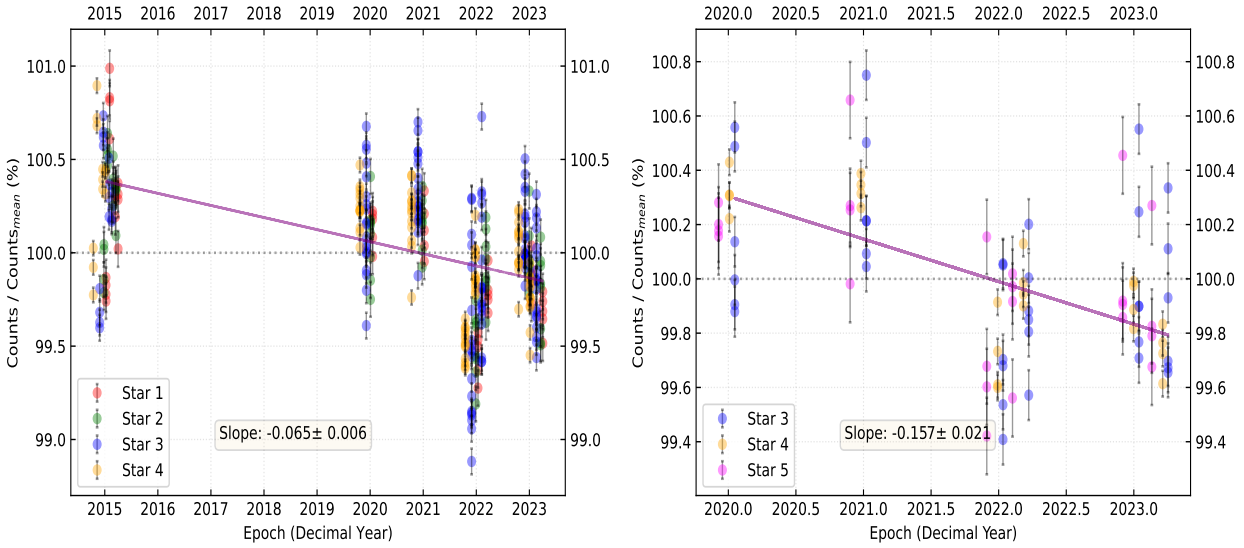

(a) (b)

Figure 3: *(a): Estimation of the time dependence of WFC3/IR imaging mode sensitivity using 10 epochs of spatial scanning observations with F140W from programs 14020, 16031, 16439, and 17261. Measurements from each star, presented relative to the mean over all ten epochs, are plotted against time. Data for the different stars from a given epoch are plotted with small artificial time offsets between them for display purposes only. The mean photometry is represented by the level at 100% (black dotted line). The solid purple line represents a linear fit to the data. The corresponding slope, quantifying the rate of sensitivity evolution is also shown. (b): Same as Fig. 3a, but with F098M data distributed over six epochs from programs 16031, 16439, and 17261.*

ascertaining the stability of the evolution rates presented here, especially the measurement for F098M from data spanning only a ∼3 year interval, requires expanding the baselines through continued monitoring.

Scanned imaging observations with F098M and F140W reveal that the sensitivity of WFC3/IR imaging mode is evolving more rapidly than several previous estimations based on staring mode observations (e.g., Kalirai, *et al.* 2011; Bajaj, *et al.* 2020) but the loss rates are less steep compared to those reported by Kozhurina-Platais & Baggett, (2020), measured using stars in the crowded core of ω-Cen. The spatial scanning estimates, however, are in 1–2 σ agreement with the spectrophotometric measurements from the IR grisms presented in section 3.

3 G102 and G141 Grisms

Beginning soon after the commissioning of WFC3 in 2009, regular monitoring of the G102 and G141 grism sensitivity includes 216 observations of the CALSPEC (Bohlin & Deustua 2019) standard stars for each grism in the stare (not scanned) mode. There are a few early spectra of G191B2B, but the current set of monitoring data is now limited to GD153, GD71,

and GRW+70°5824. The two IR grisms together cover the 800–1700 nm range in the first order with spectral resolutions R=200 and 150, respectively for G102 and G141. Spectra of these stars, extracted with an aperture height of six pixels (0.78 arcsec), were binned over the region of peak sensitivity for each grism: 850–1100 nm for G102 and 1160–1600 nm for G141, and the grism sensitivity losses were derived from a linear fit to the relative photometry as a function of time. A description of the IDL code for extraction of the grism signal versus wavelength is in Bohlin & Deustua (2019); and a Python version of the code resides in GitHub[4]. After correcting for the countrate non-linearity of 0.72% dex^{-1} (Riess, *et al.* 2019), Figures 4 and 5 show the sensitivity trends with time, and reveal loss rates of 0.115 ± 0.008% yr^{-1} for G102 and 0.061 ± 0.007% yr^{-1} for G141. These updated estimates are lower than the loss rates reported by Bohlin & Deustua (2019) of 0.169 ± 0.015% yr^{-1} (G102) and 0.085 ± 0.014% yr^{-1} (G141) which were based on a shorter baseline of observations.

Typically, these standard star observations have three dither positions for each grism in each visit and are spaced over the whole detector with an X-postarg range of -71 to +42 and a Y-postarg range of -59 to +50 arcsec. Consequently, the rms scatter seen in Figures 4 and 5 includes uncertainties in the flat-field correction. If a standard reference location is established on the detector, the precision of stellar SEDs could be improved. For example, the GRW+70°5824 observations all have X- and Y-postargs within 3.5 arcsec of zero; and the rms scatter is 0.33% and 0.35% for G102 and G141, respectively, compared to 0.47% and 0.41% for the whole ensemble.

WFC3/IR sensitivity evolution rates revealed by G102 and G141 observations closely match the corresponding estimates of -0.157 ± 0.021% yr^{-1} and -0.065 ± 0.006% yr^{-1} from spatial scans in F098M and F140W, respectively. For a more direct comparison with the scanned imaging observations, grism sensitivity loss rates were also determined from spectra binned over wavelength ranges closely approximating F098M and F140W bandpasses (Marinelli, *et al.* 2024, in prep). G102 data binned over the 850–1000 nm range reveal decreasing sensitivity at 0.116 ± 0.008% yr^{-1}, within $\sim 1.8\ \sigma$ of the loss rate estimated for F098M. Similarly, G141 spectra binned over 1160–1600 nm suggest sensitivity evolution of -0.061 ± 0.007% yr^{-1}, consistent with the measurements for F140W. The sensitivity loss rates, determined from both scanned imaging and grism observations, appear to be higher for shorter wavelengths.

4 Summary

This work investigates the long term photometric stability of WFC3/IR and provides independent estimates of the sensitivity evolution rate using spatial scanning and grism observations. High-precision photometry derived from scanned images of stars in the open cluster M35 yields the first estimate of sensitivity evolution in F098M at a rate of -0.157 ± 0.021% yr^{-1}. Spatial scanning of the same M35 field obtained over ~ 8 years provides an updated estimate of the sensitivity evolution in F140W at a rate of 0.065 ± 0.006% yr^{-1}. G102 and G141 observations of CALSPEC spectrophotometric standard stars obtained over ~ 14 years reveal sensitivity evolution rates of -0.115 ± 0.008% yr^{-1} and -0.061 ± 0.007% yr^{-1}, respectively. This work finds that the sensitivity evolution rates, estimated independently for

[4]https://github.com/spacetelescope/ABSCAL

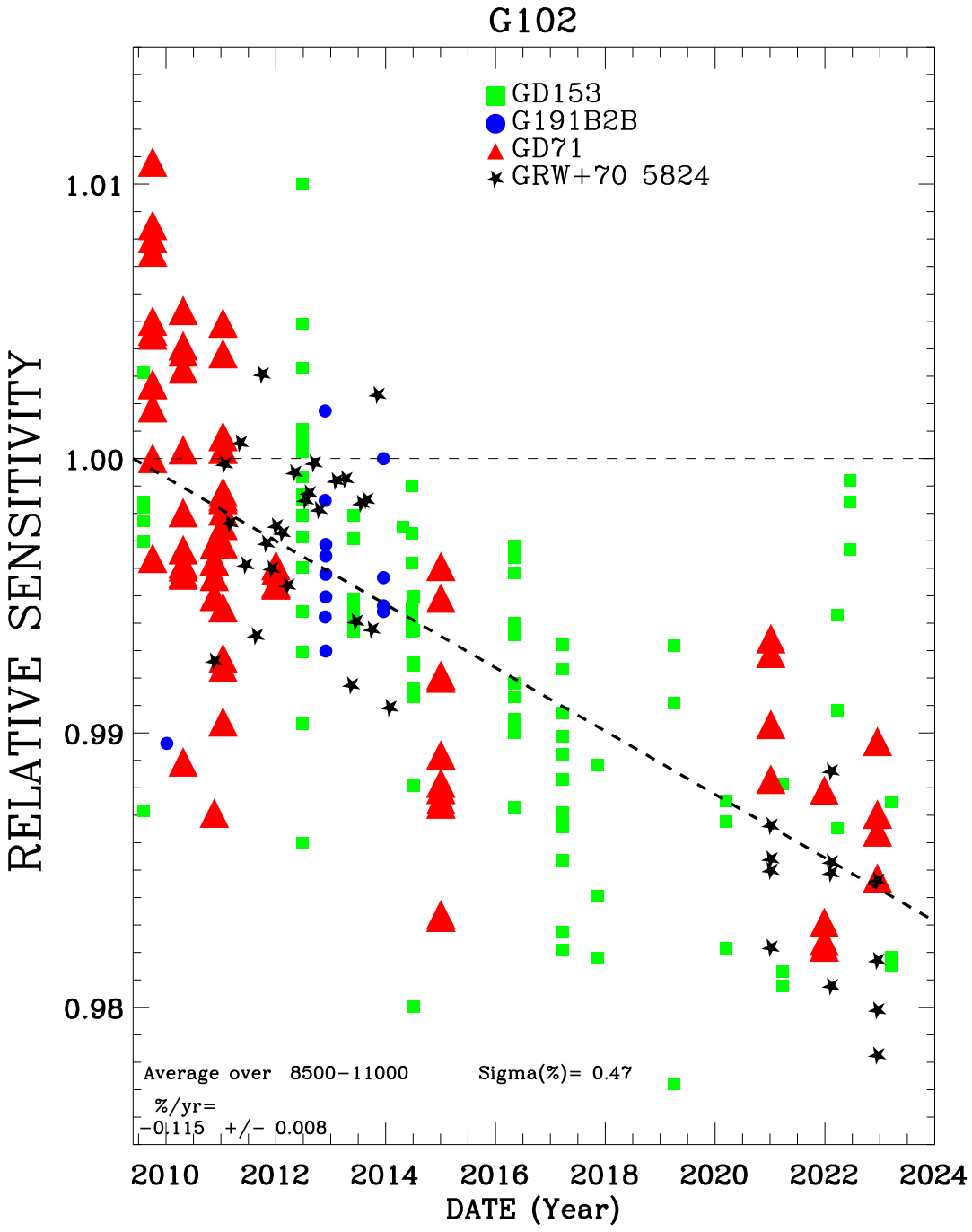

Figure 4: Change in sensitivity with time since 2009 for the WFC3 G102 grism from observations of CALSPEC standard stars, after correction for non-linearity. The current best fit loss rate is $0.115 \pm 0.008\%$ yr^{-1} and the rms residual scatter is 0.47%. The spectral binning covers most of the sensitive region from 850–1100 nm. The rms scatter is a measure of the repeatability, i.e. the 1σ broadband uncertainty in an individual observation. The least-square fit (dashed line) and the data points are all normalized to unity at 2009.4 by dividing by the initial value of the fit at 2009.4.

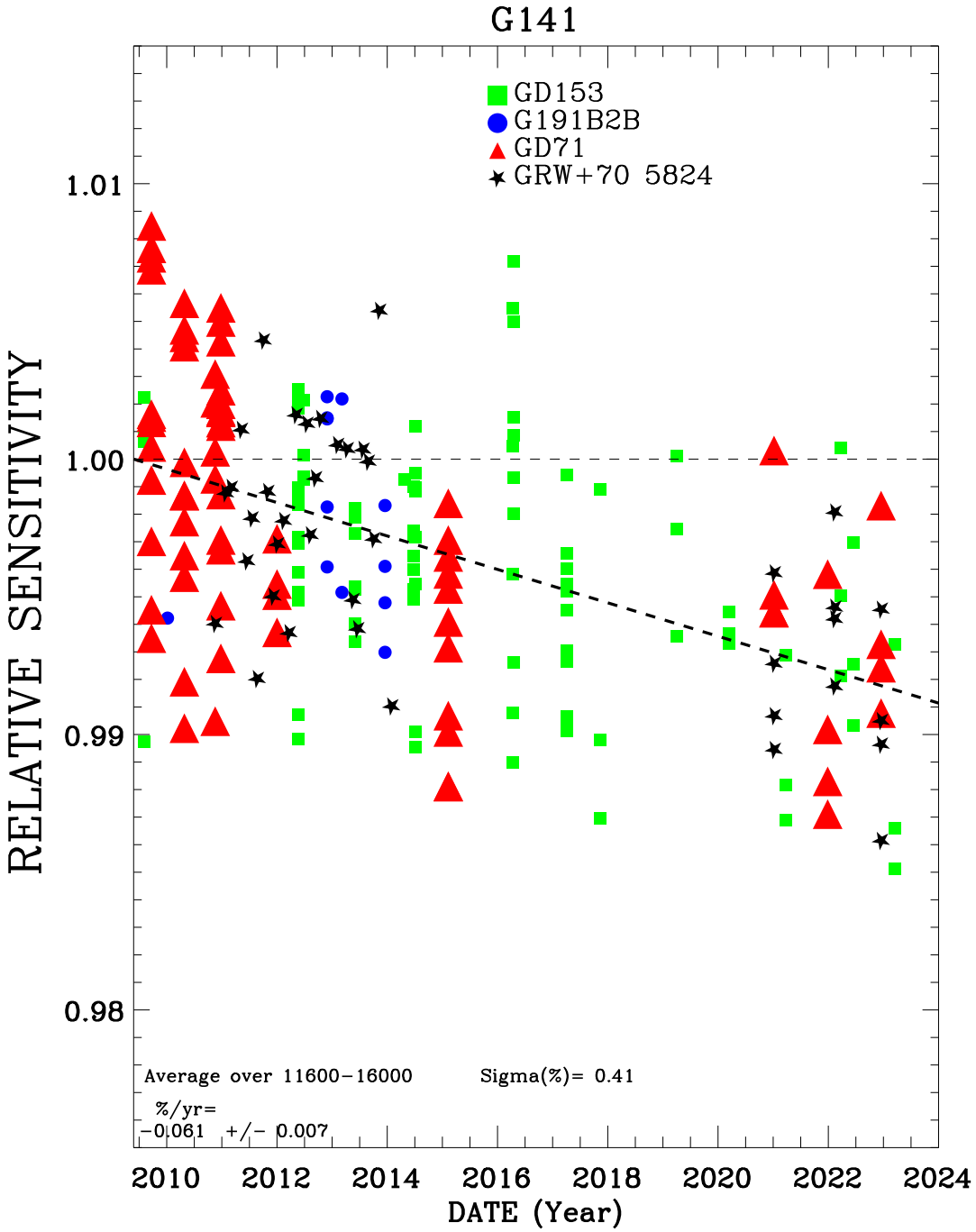

Figure 5: Change in sensitivity with time since 2009 for the WFC3 G141 grism after correction for non-linearity as in Figure 4. The current best fit loss rate is $0.061 \pm 0.007\%\ yr^{-1}$ and the rms residual scatter is 0.41%. The spectral binning covers most of the sensitive region from 1160–1600 nm.

the imaging and the grism modes of WFC3/IR, are consistent within 1–2 σ for comparable wavelength regimes. The results also suggest a wavelength dependence of the sensitivity loss but this trend requires further investigation including a wider selection of WFC3/IR filters.

5 Acknowledgements

We would like to thank Dr. Peter McCullough for his help in designing the basics of the analysis framework. We would like to thank Dr. Munazza Alam for providing careful review and comments which helped to improve this report. The authors would also like to thank the editor, Dr. Joel Green, and the members of the WFC3 Photometry Working Group for their valuable comments and suggestions during this report's preparation.

References

Bajaj, V., Calamida, A. & Mack, J. (2020). "Updated WFC3/IR Photometric Calibration." WFC3 ISR 2020-10.

Bajaj, V., Calamida, A., Mack, J. & Som, D. (2022). "WFC3/IR Photometric Stability Stellar Cluster Study" WFC3 ISR 2022-07.

Bohlin, R. C. & Deustua, S. E. (2019). "CALSPEC: Wide Field Camera 3 Infrared Grism Spectrophotometry." AJ, 157, 229.

Bohlin, R. C. et al. (2020). "Update of the Photometric Calibration of the ACS CCD Cameras." ACS ISR 2020-08.

Kalirai, J. et al. (2011). "The Photometric Performance of WFC3/IR: Temporal Stability Through Year 1." WFC3 ISR 2011-08.

Kozhurina-Platais, V. & Baggett, S. (2020). "WFC3 IR sensitivity over time." WFC3 ISR 2020-05.

Mack, J., Olszewski, H. & Pirzkal, N. (2021). "WFC3/IR Filter-Dependent Sky Flats." WFC3 ISR 2021-01.

Marinelli, M. et al. (2024). WFC3 ISR in preparation.

McCullough, P. & MacKenty, J. (2012). "Considerations for using Spatial Scans with WFC3." WFC3 ISR 2012-08.

Olszewski, H. & Mack, J. (2021). "WFC3/IR Blob Flats." WFC3 ISR 2021-10.

Riess, A. G., Narayan, G. & Calamida, A. (2019). "Calibration of the WFC3-IR Count-rate Nonlinearity, Sub-percent Accuracy for a Factor of a Million in Flux." WFC3 ISR 2019-01.

Som, D., Bajaj, V., Mack, J. & Calamida, A. (2021). "Photometric Repeatability and Sensitivity Evolution of WFC3/IR." WFC3 ISR 2021-05.